



**HAL**  
open science

## Highly passivating and blister-free hole selective poly-silicon based contact for large area crystalline silicon solar cells

Audrey Morisset, Raphaël Cabal, Bernadette Grange, Clément Marchat, José Alvarez, Marie-Estelle Gueunier-Farret, Sébastien Dubois, Jean-Paul Kleider

► **To cite this version:**

Audrey Morisset, Raphaël Cabal, Bernadette Grange, Clément Marchat, José Alvarez, et al.. Highly passivating and blister-free hole selective poly-silicon based contact for large area crystalline silicon solar cells. *Solar Energy Materials and Solar Cells*, 2019, 200, pp.109912. 10.1016/j.solmat.2019.109912 . hal-02308383

**HAL Id: hal-02308383**

**<https://centralesupelec.hal.science/hal-02308383v1>**

Submitted on 19 Mar 2020

**HAL** is a multi-disciplinary open access archive for the deposit and dissemination of scientific research documents, whether they are published or not. The documents may come from teaching and research institutions in France or abroad, or from public or private research centers.

L'archive ouverte pluridisciplinaire **HAL**, est destinée au dépôt et à la diffusion de documents scientifiques de niveau recherche, publiés ou non, émanant des établissements d'enseignement et de recherche français ou étrangers, des laboratoires publics ou privés.

# Highly Passivating and Blister-free Hole Selective Poly-Silicon Based Contact for Large Area Crystalline Silicon Solar Cells

Audrey Morisset<sup>a,b,c,\*</sup>, Raphaël Cabal<sup>a</sup>, Bernadette Grange<sup>a</sup>, Clément Marchat<sup>c</sup>, José Alvarez<sup>b,c</sup>, Marie-Estelle Gueunier-Farret<sup>b</sup>, Sébastien Dubois<sup>a</sup> and Jean-Paul Kleider<sup>b,c</sup>

<sup>a</sup>Univ. Grenoble Alpes, INES, F-73375 Le Bourget du Lac, France ; CEA, LITEN, Département des Technologies Solaires, F-73375 Le Bourget du Lac, France.

<sup>b</sup>Laboratoire de Génie Electrique et Electronique de Paris, CNRS UMR 8507, CentraleSupélec, Univ. Paris-Sud, Sorbonne Universités-UPMC Univ. Paris 06, F-91192 Gif-sur-Yvette Cedex, France.

<sup>c</sup>Institut Photovoltaïque d'Ile-de-France (IPVF), 30 RD 128, 91120 Palaiseau, France.

\*Corresponding author.

*E-mail address:* [audrey.morisset@cea.fr](mailto:audrey.morisset@cea.fr) (A. Morisset)

## Highlights:

- Blister-free boron-doped poly-Si layers are obtained by PECVD through optimization of the deposition temperature and gas ratio.
- The process developed is approaching the industrial standards (large area KOH-polished wafers, SiO<sub>x</sub> growth included in standard RCA cleaning, semi-industrial PECVD tool).
- High and homogeneous surface passivation properties are obtained ( $iV_{oc} = 734$  mV and  $J_0 = 7$  fA·cm<sup>-2</sup>).
- Conductive spots detected by C-AFM are not mirroring pinholes within the interfacial SiO<sub>x</sub> layer.

## **Abstract**

Passivating the contacts of crystalline silicon (c-Si) solar cells with a poly-crystalline silicon (poly-Si) layer on top of a thin silicon oxide ( $\text{SiO}_x$ ) is currently sparking interest for reducing recombination at the interface between the metal electrode and the c-Si substrate. Hole-selective poly-Si/ $\text{SiO}_x$  structures could be particularly relevant to passivate the rear side of mass-produced p-type c-Si solar cells (i.e., PERC solar cells). In this study, we elaborate on the optimization of a hole-selective passivating structure consisting of a boron-doped poly-Si layer on top of a chemically grown thin  $\text{SiO}_x$ . The poly-Si layer is prepared by Plasma Enhanced Chemical Vapor Deposition, which enables single-side deposition. However, if not optimized, this deposition technique leads to degradation of the poly-Si layer through a “blistering” phenomenon due to high hydrogen incorporation in the layer. To tackle this, a study of the interplay between process parameters and blistering is undertaken in order to obtain highly passivating and blister-free poly-Si/ $\text{SiO}_x$  structures. By addition of a hydrogenation step, the implied open circuit voltage ( $iV_{oc}$ ) provided by the structure is further improved, leading to a maximum value of 734 mV demonstrated on symmetrical samples made from large area wafers. We also conduct a Conductive-Atomic Force Microscopy (C-AFM) study with the aim of investigating the pinholes formation in the  $\text{SiO}_x$  interfacial layer that could explain the transport of free charge carriers within the poly-Si/ $\text{SiO}_x$  structure. We show that the current levels detected by C-AFM are affected by an oxide layer that grows at the poly-Si top surface. We also demonstrate that conductive spots detected by C-AFM are not likely to mirror conductive pinholes within the  $\text{SiO}_x$  layer but are rather linked to the poly-Si layer.

## **Keywords**

Crystalline silicon, solar cells, passivating contacts, poly-silicon, PECVD, C-AFM

## 1. Introduction

Industrial homojunction crystalline silicon (c-Si) solar cells reach conversion efficiencies above 21%[1]. However, to collect photo-generated charge carriers these cell structures involve localized and direct interfaces between the c-Si substrate and the metal electrodes. These interfaces are highly defective and induce photo-voltage losses because of charge carrier recombination. Moreover, for PERC solar cell structures, a lateral transport of charge carriers is needed to reach the localized metal contacts which affects the cell series resistance[2]. A way to overcome these issues is to implement a full area “passivating” contact, which consists of a highly-doped layer to ensure a good contact selectivity on top of a thin buffer layer for chemical surface passivation of the c-Si substrate. A first version of passivating contacts consisting of a highly-doped amorphous silicon (a-Si) layer on top of a thin intrinsic a-Si layer was implemented in the a-Si/c-Si heterojunction solar cell structure and enabled to reach conversion efficiency of 25.1% on a large area two-side contacted structure[3]. However, due to the presence of a-Si layers, the process temperature of heterojunction solar cells must remain below 250°C which prevents temperature-activated phenomena (as gettering of impurities or hydrogenation effects) to occur during the process, leading to the need for high quality c-Si wafers[4].

A promising way to passivate contacts while ensuring high-temperature stability is to use a highly-doped polycrystalline silicon (poly-Si) layer on top of a thin silicon oxide ( $\text{SiO}_x$ ) layer. The  $\text{SiO}_x$  layer growth (thermal or chemical) is followed by the deposition of a-Si or poly-Si layers either by Low-Pressure Chemical Vapor Deposition (LPCVD)[5–7], or by Plasma-Enhanced CVD (PECVD)[8–13]. Recently, the fabrication of poly-Si layers using Physical Vapor Deposition (PVD) was also demonstrated[14]. A consequent annealing step is performed to crystallize the deposited layer and/or activate dopants. Doping of the poly-Si layer can be performed in-situ by addition of a dopant-rich precursor gas (e.g.  $\text{B}_2\text{H}_6$  or  $\text{PH}_3$ )[8,11–13] or ex-situ (e.g. by diffusion[5,7] or ion implantation[15,16]). An additional hydrogenation process is generally performed to further enhance the surface passivation properties[11,12,17]. Poly-Si/ $\text{SiO}_x$  passivating structures demonstrated promising performances when integrated in solar cell devices with conversion efficiencies  $\geq 25.8\%$  obtained on small area devices ( $\sim 2 \times 2 \text{ cm}^2$ )[18,19]. Conversion efficiencies  $\geq 21.3\%$  were also

achieved on a large area device ( $\sim 156 \times 156 \text{ mm}^2$ ) with screen-printed metallization[7,13]. Despite the promising performances, these are some remaining challenges:

- The integration of hole-selective poly-Si/SiO<sub>x</sub> structures at the rear surface of existing mass produced p-type c-Si solar cells (i.e, PERC) could be one of the next significant evolutionary steps of the photovoltaic industry. So far, hole-selective poly-Si/SiO<sub>x</sub> structures have been mainly formed with boron-doped poly-Si layer (poly-Si(B)) and have historically demonstrated lower passivation performances compared to their phosphorus counterparts[17]. Despite recent progress achieved with poly-Si(B)/SiO<sub>x</sub> passivating structures on both planar and textured surfaces[20–22], boron (B) is suspected to cause more defects in the structure, especially at the interface with the SiO<sub>x</sub> layer[23], due to low B diffusivity in SiO<sub>x</sub> leading to B atoms piling-up at the SiO<sub>x</sub> layer[24,25].
- The use of PECVD is interesting for single-side deposition of the poly-Si layer, but also for optimizing the properties of the layer, notably by adding alloying elements like carbon or oxygen[12,26]. However, due to the H-rich precursor gases, the deposited a-Si:H layer is likely to blister, resulting in a severe degradation of the poly-Si layer after annealing[10,11]. Solving the blistering issue requires a fine tuning of the deposition conditions (especially the deposition temperature and the gas ratio)[10–12].
- The transport mechanism of charge carriers through the poly-Si/SiO<sub>x</sub> structure has recently been actively investigated but is still not fully understood yet[27–31]. Two hypothetical transport regimes have been identified: a regime of charge carriers tunneling through the SiO<sub>x</sub> layer[32], and a regime of direct transport through pinholes formed in the SiO<sub>x</sub> layer upon annealing[33]. The poly-Si/SiO<sub>x</sub> structure was notably studied by means of Conductive-Atomic Force Microscopy (C-AFM) with the aim of detecting pinholes in the SiO<sub>x</sub> layer[34,35].

This contribution focuses on poly-Si(B)/SiO<sub>x</sub> structures prepared by PECVD with the aim of integrating the structure at the rear side of a p-type c-Si solar cell (see Fig. 1). First, we address the optimization of the deposition temperature and gas ratio that enabled to obtain blister-free poly-Si(B)/SiO<sub>x</sub> structures while insuring good surface passivation properties. Surface passivation properties were improved by optimizing the annealing temperature and by addition of a post-process

hydrogenation step. Then, Conductive-Atomic Force Microscopy (C-AFM) measurements were performed to investigate the formation of conductive pinholes in the  $\text{SiO}_x$  layer. We first evaluated the impact of an oxide present at the poly-Si top surface on the current levels detected by C-AFM. We then investigated the possible link between conductive spots observed on C-AFM current maps and conductive pinholes in the  $\text{SiO}_x$  layer.

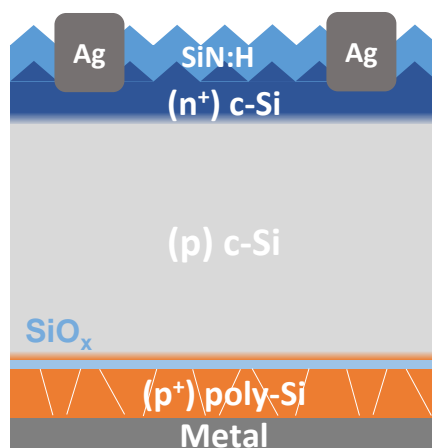


**Fig. 1.** Schematic of a p-type c-Si solar cell where the  $(p^+)$  poly-Si(B)/ $\text{SiO}_x$  structure discussed in this paper is integrated at the rear surface. The cell features a front  $(n^+)$  c-Si emitter that is coated with an anti-reflective hydrogen-rich silicon nitride layer (SiN:H). Local Ag metal contacts are formed on the front side. The rear contact consists of a full-area metal layer (e.g. Ag, Al).

## 2. Experimental

### 2.1. Sample preparation

In order to optimize the deposition parameters, single side poly-Si(B) passivating structures were fabricated using 275  $\mu\text{m}$ -thick double-side-mirror-polished 4 inch n-type Czochralski (Cz) (100) c-Si wafers (resistivity ( $\rho$ ) of 2-3  $\Omega\cdot\text{cm}$ ). A thin  $\text{SiO}_x$  layer ( $\sim 1.3$  nm) was grown on the wafers surface by integrating a 10 min-long ozonized DI- $\text{H}_2\text{O}$  rinsing in our wet chemical cleaning. A hydrogen-rich boron-doped a-Si layer (a-Si:H(B)) was single-side deposited by PECVD on top of the  $\text{SiO}_x$  layer, using a 13.56 MHz PECVD reactor. Precursor gases consisted of silane ( $\text{SiH}_4$ ), hydrogen ( $\text{H}_2$ ), and  $\text{H}_2$ -diluted diborane ( $\text{B}_2\text{H}_6$ ). The a-Si:H(B) layer thickness was targeted in the range 20-30 nm. The samples were annealed in the range 700-900°C in a tube furnace under argon atmosphere in order to

activate dopants and crystallize the a-Si:H(B) layer. Samples were loaded at 400°C with a ramp rate of ~10°C/min to reach the annealing temperature ( $T_a$ ) for a 30 min plateau and were unloaded at 700°C with a similar ramp rate down (for  $T_a > 700^\circ\text{C}$ ). In the following, we use the term “poly-Si” to refer to the layer after annealing. For the C-AFM study, samples “without interfacial  $\text{SiO}_x$ ” were prepared the same way except that the c-Si wafer was dipped in hydrofluoric acid (HF) prior to the PECVD step (delay < 5 min) in order to remove the interfacial  $\text{SiO}_x$  layer, leading to a poly-Si(B)/c-Si stack.

The effect of the poly-Si annealing temperature and hydrogenation on surface passivation properties was evaluated on symmetrical samples made from the afore-described mirror-polished 4 inch c-Si wafers and also from 180  $\mu\text{m}$ -thick KOH-polished 156 mm pseudo square (psq) n-type Cz (100) wafers ( $\rho = 6 \Omega\cdot\text{cm}$ ). The process was similar to the one previously described except that the a-Si:H(B) layer was deposited by PECVD on both sides of the wafer. The annealing step was followed by a hydrogenation step consisting of the deposition of H-rich silicon nitride layer on top of the poly-Si layer followed by a firing step in a conventional belt furnace ( $T_{\text{firing}} \sim 760^\circ\text{C}$ ). A subsequent chemical etching of the SiN:H layer was performed on these samples by dipping them in a concentrated HF solution for approximately 1 min.

## 2.2. Characterization techniques

The thickness of  $\text{SiO}_x$ , a-Si:H(B) and final poly-Si(B) layers was measured by spectroscopic ellipsometry (SE) (Jobin Yvon tool, HORIBA) on mirror-polished c-Si wafers. For the fitting model of the poly-Si(B) layer, we considered a layer consisting of a mix of crystalline clusters in an amorphous matrix (adapted from ref.[36]). The thickness of the layer measured by SE after deposition and after annealing were in good agreement with the targeted thickness (within  $\pm 2$  nm of error) so to simplify the following, only the targeted thickness will be mentioned. The imaginary part of the dielectric function obtained as a function of the photon energy through SE measurement was used to verify the amorphous nature of a-Si:H(B) layers after deposition (curve featuring a broad peak centered around 3.3 eV) and the crystallization of the poly-Si layer after annealing (curve featuring two peaks centered around 3.4 and 4.2 eV)[36].

Optical microscopic observations of the poly-Si(B) layer after annealing were performed with a BX61 tool (Olympus). The resulting images were analyzed using the software ImageJ to assess the blister diameter and density.

Electrical properties (conductivity, Hall mobility and charge carrier concentration) of the poly-Si(B) layer were evaluated by Hall effect technique (HMS-5500 tool, Ecopia) on laser cut  $2 \times 2 \text{ cm}^2$  pieces of samples. Electrochemical capacitance-voltage (ECV) measurements were carried out to estimate the majority carrier (approximated as the active boron) concentration profile in the poly-Si(B) layer using a ECV WEP CVP21 tool with a  $0.1 \text{ mol/l NH}_4\text{F}$  solution as etchant.

The effective carrier lifetime was measured by photo-conductance decay (PCD) technique using a WCT 120 tool (Sinton Instruments), in order to obtain the implied open circuit voltage ( $iV_{oc}$ ) and the recombination current density ( $J_0$ ) (extracted using the method of Kane and Swanson[37]). The surface passivation properties provided by the poly-Si(B)/SiO<sub>x</sub> structure were evaluated on symmetrical samples fabricated from mirror-polished 4 inch c-Si wafers and from 156 psq KOH-polished c-Si wafers. On the latter, we performed a five-point mapping of the PCD measurement (one measurement in the center and four measurements at approximately 4 cm of the edges) to evaluate the spatial homogeneity of surface passivation properties after annealing. The PCD measurement was also performed after SiN:H chemical etching.

Conductive atomic force microscopy (C-AFM) measurements were carried out with an AFM Combiscope AIST-NT (HORIBA) with an integrated Resiscope module on samples made from mirror-polished c-Si wafers. C-AFM measurements were conducted in contact mode using PtSi-FM tips (Nanosensors) placed at the poly-Si(B) surface, under air and dark conditions. A polarization of -1 V was applied between the tip and the second contact. C-AFM measurements were performed in two different configurations:

- In transversal configuration i.e. the voltage was applied between the AFM tip and a silver contact located at the back side of the c-Si.
- In lateral configuration i.e. the voltage was applied between the AFM tip and a silver contact localized at the poly-Si(B) surface (resulting in a short-circuit of the layer).



The resulting current maps were analyzed using the software ImageJ to assess the density of conductive spots.

### **3. Results and discussion**

#### *3.1. Optimization of the poly-Si(B)/SiO<sub>x</sub> structure*

##### *3.1.1 Blistering reduction*

Several studies have shown that poly-Si/SiO<sub>x</sub> structures fabricated by PECVD of a-Si:H layer on top of SiO<sub>x</sub> are prone to blistering[10–12]. The blistering phenomenon is observed during the deposition of the a-Si:H layer and also during the annealing step to form poly-Si. Even though a fundamental understanding of the phenomenon is still lacking, some hypotheses have been proposed. Blistering during PECVD might be related to adhesion properties of the a-Si:H film to the SiO<sub>x</sub> layer coupled with a high amount of H incorporated in the layer, leading to the accumulation of H<sub>2</sub> molecules at the a-Si:H(B)/SiO<sub>x</sub> interface[38]. Blistering during the annealing step is likely due to rapid release of H<sub>2</sub> at high temperature[39]. As a consequence, a severe degradation of the final poly-Si(B) layer is observed if the deposition and annealing conditions are not optimized[10,11].

In this part we address the optimization of the PECVD parameters in order to minimize the incorporation of H in the a-Si:H(B) layer, reducing therefore blistering of the final poly-Si(B) layer. In all the work presented here, the annealing step was performed by placing the samples in the furnace at low temperature (400°C) followed by a slow ramp-up rate (~10°C/min) to reach the targeted annealing temperature (T<sub>a</sub>) in order to mitigate blistering during annealing. As a first step, 30 nm-thick a-Si:H(B) layers were deposited on top of SiO<sub>x</sub> using a deposition temperature T<sub>dep</sub> = 220°C and a gas ratio R = H<sub>2</sub>/SiH<sub>4</sub> = 6 which resulted in a severe blistering of the layer after both deposition and annealing at T<sub>a</sub> = 700°C (see Fig. 2). The first way to minimize the incorporation of H in the a-Si:H(B) layer was to increase the deposition temperature (T<sub>dep</sub>) leading to the reduction of H incorporation in the deposited layer[39,40]. In this study, the increase of T<sub>dep</sub> from 220°C to 300°C (limit of the PECVD equipment) enabled to reduce the blister diameter from 20 μm to 8 μm after deposition and from 30 μm to 13 μm after annealing (Fig. 2, Step 1), however, the blister density remained unchanged (1.5 mm<sup>-2</sup>).

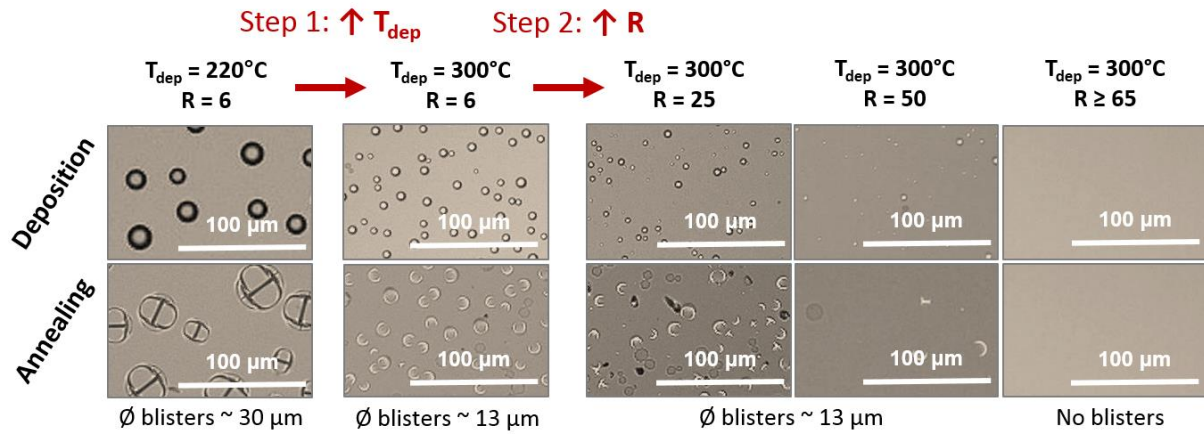


**Fig. 2.** Optical microscope images of 30 nm-thick poly-Si(B) layers after deposition and after annealing at 700°C (at a  $\times 20$  magnification). The deposition conditions were varied: **Step 1.** Increase of the deposition temperature  $T_{\text{dep}}$ , **Step 2.** Increase of the gas flow ratio  $R = \text{H}_2/\text{SiH}_4$ . For each set of conditions, the diameter of the blisters ( $\emptyset$  blisters) and their density were evaluated.

The second way to reduce the blistering was to increase the gas flow ratio  $R = \text{H}_2/\text{SiH}_4$  during the deposition step[11]. It is to note that high  $R$  during the PECVD step could lead to microcrystalline deposited layers, however, as the deposited layer was in-situ doped with B, it remained amorphous (which was verified by spectroscopic ellipsometry (SE))[41]. The increase of  $R$  led to a reduction of the blister density after deposition and after annealing from  $1.5 \text{ mm}^{-2}$  to  $0.6 \text{ mm}^{-2}$  for  $R$  from 6 to 50 respectively (Fig. 2, Step 2). Increasing  $R$  to 65 enabled to obtain blister-free poly-Si(B) layers. Fig. 3a depicts the deposition rate as a function of the gas ratio  $R$ . Increasing  $R$  led to the decrease of the deposition rate which is assumed to promote H atoms diffusion toward the top surface of the layer during the deposition step, thus mitigating the blistering phenomenon. Fig. 3a also depicts the  $iV_{\text{oc}}$  (assessed on mirror-polished samples) as a function of the gas ratio  $R$ . For  $R = 25$  to  $R = 50$ , an increase of  $iV_{\text{oc}}$  of 90 mV was observed, concomitantly to blistering reduction. When further increasing  $R$  to 65, a drop of 20 mV in  $iV_{\text{oc}}$  was observed. This drop was attributed to the excessive  $\text{H}_2$  concentration in the plasma causing radiation induced charges in the  $\text{SiO}_x$  layer[42,43]. An optimal gas ratio of  $R = 50$  was found to reduce the blister density ( $0.6 \text{ mm}^{-2}$  for a poly-Si thickness of 30 nm) and preserve decent  $iV_{\text{oc}}$  after annealing at 700°C. The remaining blistering was avoided by decreasing the

thickness of the poly-Si(B) from 30 nm to 20 nm which resulted in blister-free layers for the optimal deposition conditions  $T_{\text{dep}} = 300^\circ\text{C}$  and  $R = 50$ .

In this paragraph, we address the evaluation of the conductivity and carrier mobility of the poly-Si layer over  $T_{\text{dep}}$  and  $R = \text{H}_2/\text{SiH}_4$  optimizations. The lateral conductivity and carrier mobility of 30 nm-thick poly-Si(B) layers were evaluated by Hall effect measurements as function of  $T_{\text{dep}}$  and  $R$  (see Fig. 3b). Hall effect measurements were performed on samples annealed at  $T_a = 700^\circ\text{C}$  to ensure a negligible B in-diffusion in the c-Si (see Fig. 4). For the different  $T_{\text{dep}}$  and  $R$  conditions investigated, the Hall carrier density was measured constant at  $1.1 \pm 0.2 \times 10^{20} \text{ cm}^{-3}$ . As a consequence, the conductivity trend was dominated by the carrier mobility in the layer (see Fig. 3b). The poly-Si(B) conductivity increased from  $160 \text{ S}\cdot\text{cm}^{-1}$  for  $T_{\text{dep}} = 220^\circ\text{C}$  and  $R = 6$  to  $220 \text{ S}\cdot\text{cm}^{-1}$  for  $T_{\text{dep}} = 300^\circ\text{C}$  and  $R = 50$ . This increase is likely to result from the reduction of the poly-Si(B) blistering leading to a better lateral transport of charge carriers through the layer.

In conclusion, the optimization of the deposition temperature and gas ratio enabled to reduce the blistering of 30 nm-thick poly-Si layer. A further reduction of the poly-Si thickness to 20 nm enabled to obtain blister-free poly-Si(B) layers. In the following, the poly-Si(B) layer was systematically deposited with  $T_{\text{dep}} = 300^\circ\text{C}$ ,  $R = 50$  and targeting a thickness of 20 nm to obtain blister-free layers. A sheet resistance value of 1300 ohm/sq was evaluated by four probe measurement on the 20 nm-thick poly-Si layer.

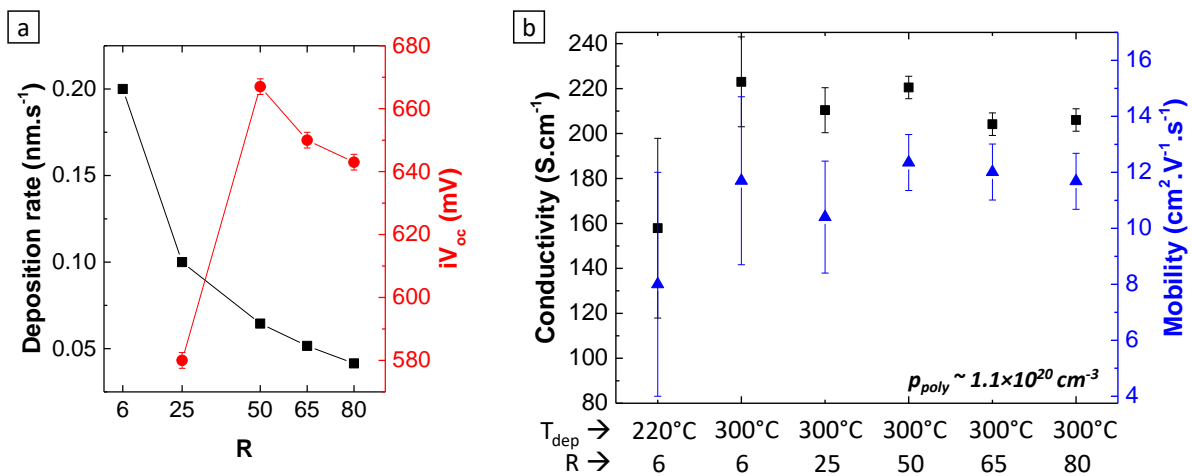


**Fig. 3.** Deposition rate of the a-Si:H(B) layer and *iV*<sub>oc</sub> (measured on symmetrical samples made from mirror-polished c-Si wafers) as a function of the gas flow ratio  $R = \text{H}_2/\text{SiH}_4$  (a). Conductivity and carrier

mobility of 30 nm-thick poly-Si(B) layers measured by Hall effect technique as function of the deposition temperature ( $T_{\text{dep}}$ ) and gas ratio (R) optimizations (b). Samples were annealed at  $T_a = 700^\circ\text{C}$ . The carrier density of poly-Si(B) layers ( $p_{\text{poly}}$ ) was evaluated by Hall effect measurement and was constant with an average value of  $1.1 \pm 0.2 \times 10^{20} \text{ cm}^{-3}$ .

### 3.1.2 Impact of annealing temperature on surface passivation properties

In this part we address the impact of the annealing temperature ( $T_a$ ) on the resulting poly-Si(B)/SiO<sub>x</sub> surface passivation properties. Several studies evidenced an optimal  $T_a$  to maximize the surface passivation provided by the poly-Si(B)/SiO<sub>x</sub> structure. This optimum corresponds to a trade-off between two T-activated phenomena:

- The shallow in-diffusion of dopants from the poly-Si layer to the c-Si substrate, which enhances the field-effect passivation at the c-Si surface[44,45]
- The degradation of the interfacial SiO<sub>x</sub> layer which decreases the chemical passivation properties (interface state density ( $D_{\text{it}}$ ) increase)[17,46,47]

The poly-Si(B)/SiO<sub>x</sub> samples were first fabricated on mirror polished c-Si wafers. The a-Si:H(B) layer was deposited with optimized deposition conditions ( $T_{\text{dep}} = 300^\circ\text{C}$  and  $R = 50$ ). Samples were then annealed at  $T_a = 700^\circ\text{C}$ ,  $800^\circ\text{C}$  or  $900^\circ\text{C}$ . The crystalline nature of the poly-Si layer after annealing was verified by SE. A poly-Si(B) thickness of 20 nm was targeted, resulting in blister-free layers after annealing. For each  $T_a$ , the active B concentration profile of the poly-Si(B) layer was measured by ECV, the resulting profiles are depicted in Fig. 4.

For  $T_a = 700^\circ\text{C}$ , the Hall effect measurement resulted in a Hall carrier density of  $1.3 \pm 0.2 \times 10^{20} \text{ cm}^{-3}$ . From the B concentration profile obtained by ECV in the poly-Si(B) layer, a carrier density of  $1.7 \pm 0.1 \times 10^{20} \text{ cm}^{-3}$  was evaluated which is in good agreement with the Hall carrier density. The increase of  $T_a$  to  $800^\circ\text{C}$  and  $900^\circ\text{C}$  resulted in a significant B in-diffusion in the c-Si substrate (30 nm and 160 nm-deep, respectively). As a consequence, the evaluation of the poly-Si(B) electrical properties via Hall effect measurement was not possible due to the current flowing in the p<sup>+</sup>-doped part of the c-Si.

For each  $T_a$ , surface passivation properties were evaluated, the resulting  $iV_{oc}$  values are indicated in Fig. 4, with their associated B concentration profiles. An optimal  $T_a$  of 800°C was found to maximize the  $iV_{oc}$  value to 690 mV and minimize the  $J_0$  value to 30 fA/cm<sup>2</sup>. When increasing  $T_a$  up to 900°C a decrease of  $iV_{oc}$  to 630 mV was observed as well as an increase of  $J_0$  to 260 fA/cm<sup>2</sup>, attributed to the combination of the deep B in-diffusion in the c-Si and the degradation of the SiO<sub>x</sub> interfacial layer.

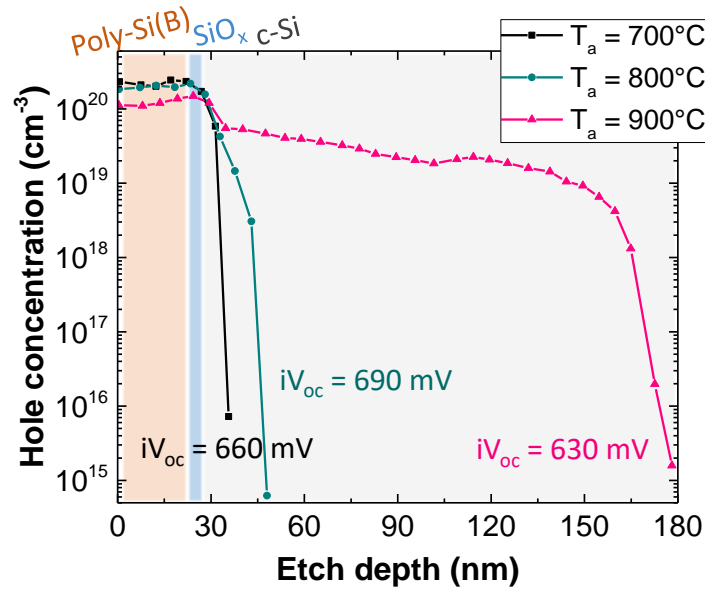


**Fig. 4.** Hole concentration (approximated as the active boron) profiles measured by electrochemical capacitance-voltage (ECV) on samples annealed at different temperatures ( $T_a$ ).

Using the same deposition conditions we studied the impact of  $T_a$  on surface passivation of 156 psq KOH-polished c-Si wafers, which corresponds to the area and topography targeted for device integration of the poly-Si(B)/SiO<sub>x</sub> passivating structure. Fig. 5 depicts the average  $iV_{oc}$  and  $J_0$  values measured after annealing as function of  $T_a$  in the range 700 – 850°C (on five samples per  $T_a$  value investigated). A similar trend as in the case of mirror-polished samples was observed: from  $T_a = 700^\circ\text{C}$  to  $800^\circ\text{C}$  the  $iV_{oc}$  value increased from 661 mV to 689 mV respectively. For  $T_a = 850^\circ\text{C}$ , the  $iV_{oc}$  value dropped to 664 mV. An optimal  $T_a$  value of 800°C was found to maximize  $iV_{oc}$  and minimize  $J_0$  after annealing. The PCD technique was performed on 5 points per sample to evaluate the spatial homogeneity of the surface passivation properties after annealing. A spatial dispersion of 3 mV and 2.5 fA·cm<sup>-2</sup> was evaluated for  $iV_{oc}$  and  $J_0$  respectively, showing the good homogeneity of the poly-Si(B)/SiO<sub>x</sub> fabrication process on large area wafers.

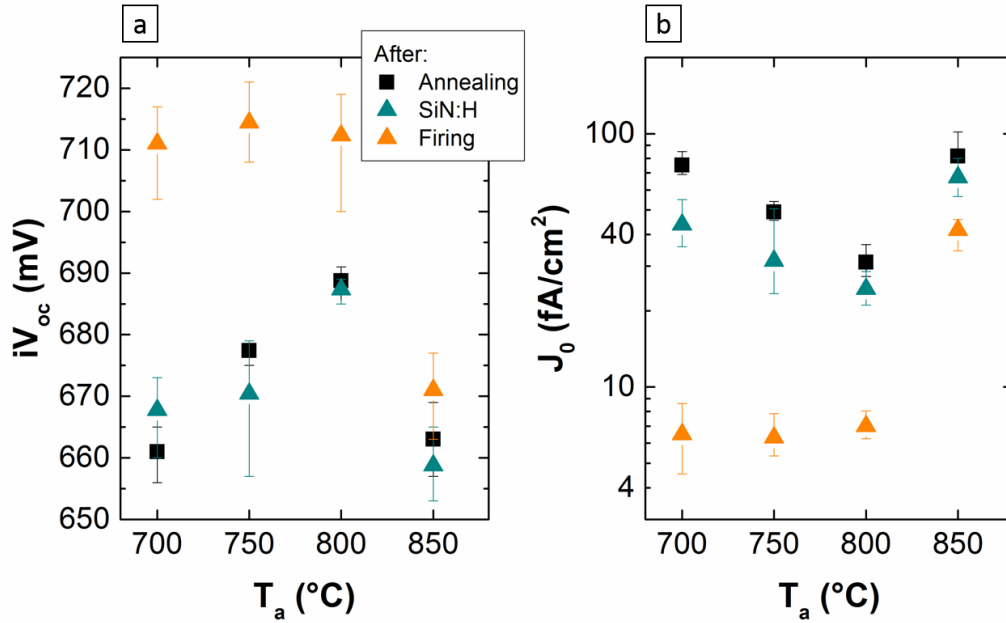


**Fig. 5.** Surface passivation properties ( $iV_{oc}$  (a) and  $J_0$  (b)) provided by the poly-Si(B)/SiO<sub>x</sub> structure as function of the annealing temperature  $T_a$ , evaluated on symmetrical samples (made from KOH-polished 156psq c-Si wafers) after annealing, SiN:H deposition and firing ( $d_{poly} = 20$  nm).

### 3.1.3 Impact of the hydrogenation step

The surface passivation properties provided by the poly-Si(B)/SiO<sub>x</sub> structure fabricated on KOH-polished c-Si wafers were further improved by depositing a hydrogenated silicon nitride (SiN:H) layer on top of the poly-Si(B) (both sides), followed by a firing step. The resulting  $iV_{oc}$  and  $J_0$  values measured after SiN:H deposition and after a subsequent firing step are plotted in Fig. 5. The SiN:H deposition did not impact significantly the  $iV_{oc}$  value over the entire  $T_a$  range although slightly decreasing the  $J_0$  values. For every sample annealed at  $T_a \leq 800^\circ\text{C}$ , performing a subsequent firing step resulted in an increase of  $iV_{oc}$  above 700 mV as well as a decrease of  $J_0$  below 10 fA·cm<sup>-2</sup>. A maximum  $iV_{oc}$  of 721 mV was reached for  $T_a = 750^\circ\text{C}$ , corresponding to a  $J_0$  value of 5.3 fA·cm<sup>-2</sup>. After firing, one can note that the lower the  $T_a$  the greater the absolute gain in  $iV_{oc}$  and  $J_0$ .

By fabricating similar samples using better quality KOH-polished 156psq n-type Cz c-Si wafers, an average  $iV_{oc}$  of 731 mV was obtained after annealing at  $T_a = 700^\circ\text{C}$  with a best value of 734 mV (corresponding to a  $J_0$  of 7 fA·cm<sup>-2</sup>). This is among the best values obtained so far with p<sup>+</sup>-poly-Si

symmetrical samples on planar surface (in the range 732-735 mV for  $iV_{oc}$  and 1-10  $fA \cdot cm^{-2}$  for  $J_0$ )[14,20,21,23]. Values of 720 mV and 10  $fA \cdot cm^{-2}$  were also demonstrated on textured surface[22].

As mentioned in the introduction, we aim to integrate the poly-Si(B)/SiO<sub>x</sub> structure at the rear side of a p-type solar cell with a full area rear metallization[14] (see Fig. 1), which implies the removal of the SiN:H layer prior to metal deposition. After chemical etching of the SiN:H layer, the surface passivation properties remained good on all the  $T_a$  range investigated ( $iV_{oc}$  average loss < 4 mV).

### 3.2 Investigation of transport mechanisms within the interfacial oxide

The transport mechanism of charge carriers through the poly-Si/SiO<sub>x</sub> structure has recently been actively investigated[27–31]. It has been found to be process dependent and two hypothetical transport regimes have been identified: a regime of charge carriers tunneling through thin SiO<sub>x</sub> layer (< 2 nm) exposed to moderate temperature annealing ( $T_a < 800^\circ C$ )[32], and a regime of direct transport through pinholes formed in the SiO<sub>x</sub> layer upon annealing, generally achieved by growing a thicker SiO<sub>x</sub> layer (> 2 nm) and exposed to high temperature annealing ( $T_a > 1000^\circ C$ )[33]. C-AFM measurements on poly-Si/SiO<sub>x</sub> structures have been reported in the literature with the aim of detecting the presence of pinholes in the SiO<sub>x</sub> layer[34,35]. Localized regions of higher current intensity (conductive spots) were observed on the resulting C-AFM current maps. However, a clear link between these conductive spots and the presence of pinholes within the SiO<sub>x</sub> layer has not been established yet.

In the present study, we first evaluated the impact of an oxide present at the poly-Si top surface on the current levels detected by C-AFM. Then, we investigated the link between conductive spots observed on C-AFM current maps and the presence of pinholes in the interfacial SiO<sub>x</sub> layer by performing measurements in different configurations (transversal or lateral), with and without SiO<sub>x</sub> layer at the poly-Si/c-Si interface.

#### 3.2.1 Impact of the surface oxide on the C-AFM measurement

Despite the inert atmosphere imposed during the annealing step, an oxide layer of approximately 3 nm was measured by SE at the surface of our samples (i.e. at the poly-Si(B) top surface) probably

due to the tube furnace used during annealing which is not being sealed (no load lock). A preliminary study consisted in evaluating the impact of this oxide on the current levels detected by C-AFM.

A first C-AFM measurement was performed in transversal configuration (i.e. the voltage was applied between the AFM tip and a contact located at the back side of the c-Si) on a sample featuring a 20 nm-thick poly-Si(B) layer annealed at 700°C (deposited on n-type mirror-polished c-Si wafer). The oxide at the poly-Si(B) top surface was then removed through a HF-cleaning step and followed by several transversal C-AFM measurements performed from 30 min to 5h after HF-cleaning, the samples being stored under air in the meantime. The resulting current maps measured after annealing and at different times after HF-cleaning are depicted in Fig. 6. From the current maps, the surface distribution of the detected current was extracted (Fig. 7). After annealing, the current distribution curve features a peak at 3.9 pA corresponding to the mean current intensity ( $I_{\text{mean}}$ ) and a maximum current intensity ( $I_{\text{max}}$ ) detected at 5.8 nA. The C-AFM measurement performed 30 min after HF-cleaning showed an increase of  $I_{\text{mean}}$  and  $I_{\text{max}}$  up to 0.25 nA and 114.7 nA respectively. The C-AFM measurement performed 2h after the HF-cleaning step showed then a decrease of  $I_{\text{mean}}$  and  $I_{\text{max}}$  (down to  $4.9 \times 10^{-2}$  nA and 88.7 nA respectively) due to the re-growth of an oxide layer at the sample's surface. The measurement performed 5h after cleaning showed similar values of  $I_{\text{mean}}$  and  $I_{\text{max}}$  than after 2h, indicating that the surface oxide layer did not evolve significantly in between these two measurements.

These results emphasized the impact of the oxide at the surface of the samples after annealing that decreased the current levels detected by C-AFM. To avoid any misinterpretation due to a different surface state, C-AFM measurements presented in the following part were performed with a constant delay between the HF-cleaning and the measurement.



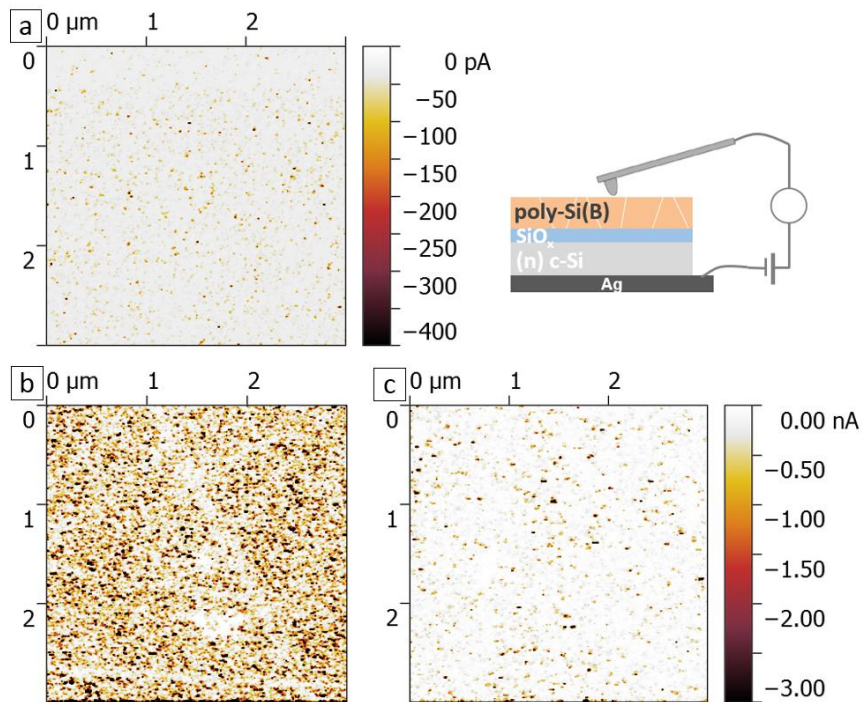


**Fig. 6.** Current maps obtained by C-AFM measurement in transversal configuration on a 20 nm-thick poly-Si(B) layer annealed at 700°C (a) and at different times after HF-cleaning the poly-Si(B) surface (30 min (b) and 5h (c)).

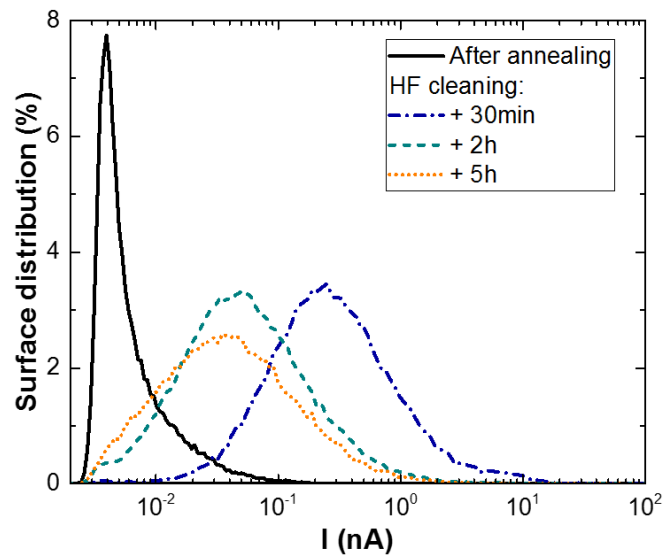


**Fig. 7.** Surface distribution of the detected currents extracted from C-AFM current maps measured at the poly-Si(B) surface in transversal configuration after annealing at 700°C and at different times after HF-cleaning the poly-Si(B) surface (from 30min to 5h).

### 3.2.2 C-AFM investigation of the pinholes formation within the $\text{SiO}_x$ layer

C-AFM measurements performed on poly-Si/SiO<sub>x</sub> structures result in the detection of localized regions of higher current intensity (conductive spots). Moreover, Lancaster et al. detected higher current levels when performing C-AFM on poly-Si/SiO<sub>x</sub> structures annealed at 950°C than on structures annealed at 800°C[34]. They proposed that this observation could result from a lower resistance of the SiO<sub>x</sub> layer as the density of pinholes in the SiO<sub>x</sub> layer has been observed to increase with increasing T<sub>a</sub>[48]. To investigate the possible link between these conductive spots and pinholes in the interfacial SiO<sub>x</sub> layer, C-AFM measurements were performed on samples annealed at different temperatures. 20 nm-thick poly-Si(B) layers were deposited with optimized conditions (T<sub>dep</sub> = 300°C and R = 50) on n-type mirror-polished c-Si wafers. The annealing temperature was varied in the range 700°C to 900°C. C-AFM measurements were performed with a constant delay of 2h after HF-cleaning the samples' surface. Fig. 8a and Fig. 8b depict current maps obtained in transversal configuration on poly-Si layers annealed at 700°C and 900°C. The density of conductive spots (> 1 nA) was found to increase from 55 μm<sup>-2</sup> to 215.4 μm<sup>-2</sup> respectively. The current levels were found to increase with increasing T<sub>a</sub> from 700°C to 900°C which is in good agreement with observations of Lancaster et al.[34], and could result from a lower electrical resistance of the SiO<sub>x</sub> layer due to conductive pinholes forming in the layer upon annealing at higher T<sub>a</sub>. Moreover, the increase of the conductive spots density with increasing T<sub>a</sub> is consistent with the increase of pinhole density with increasing T<sub>a</sub>[48] and could lead to the hypothesis that the conductive spots detected by C-AFM are mirroring pinholes within the interfacial SiO<sub>x</sub> layer.

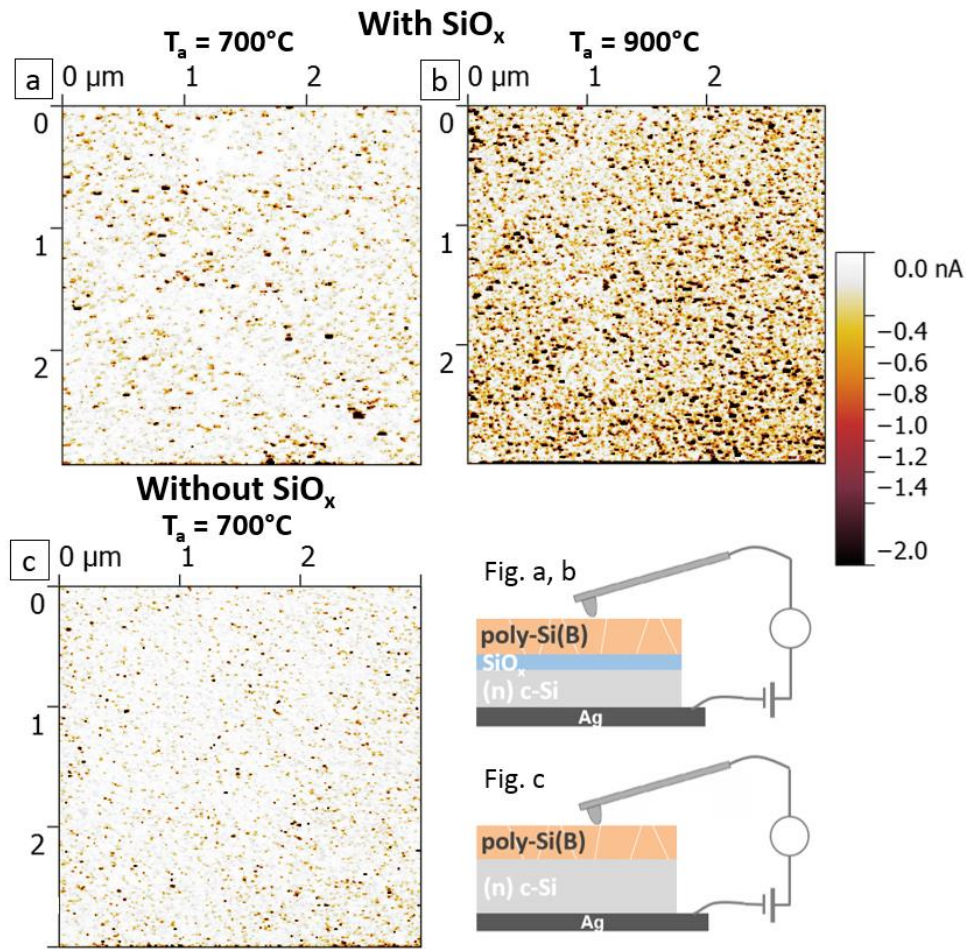


Fig. 8. Current maps obtained by C-AFM measurement in transversal configuration at the surface of samples with an intentionally grown  $\text{SiO}_x$  layer at the poly-Si(B)/c-Si interface after annealing at  $700^\circ\text{C}$  (a) and at  $900^\circ\text{C}$  (b). The same measurement was performed on a sample without interfacial  $\text{SiO}_x$  layer (annealed at  $700^\circ\text{C}$ ) (c). C-AFM measurements were systematically performed 2h after HF-cleaning the samples' surface to ensure a similar surface state during the measurement.

To further investigate the correlation between conductive spots and pinholes in the  $\text{SiO}_x$  layer, we performed C-AFM measurements on a sample featuring a similar poly-Si(B) layer without interfacial  $\text{SiO}_x$  layer. This sample was fabricated by dipping the c-Si wafer in HF prior to the a-Si deposition step in order to remove the interfacial  $\text{SiO}_x$  layer, leading to a poly-Si/c-Si stack ( $T_a = 700^\circ\text{C}$ ). The C-AFM measurement was performed 2h after HF-cleaning the sample's surface. The pattern of the resulting current map was similar to the one obtained in the case of an intentionally grown interfacial  $\text{SiO}_x$  layer (Fig. 8a), with a density of conductive spots in the same range ( $50.8 \mu\text{m}^{-2}$ , Fig. 8c).

However, lower current levels were detected, although the resistance of the poly-Si/c-Si stack was expected to be lower due to the absence of interfacial SiO<sub>x</sub> layer. The slightly lower current levels obtained could result from a larger resistance of the poly-Si layer as the crystalline structure of the poly-Si layer is expected to depend on the surface state of the c-Si wafer (oxidized or HF-cleaned) before deposition. Despite the lower current levels, the detection of conductive spots when performing C-AFM measurements on a sample without interfacial SiO<sub>x</sub> layer is disproving the hypothesis that conductive spots could mirror pinholes in the SiO<sub>x</sub> layer.

To further investigate on the conductive spots observed on current maps, additional C-AFM measurements were performed on similar samples in lateral configuration (i.e. the voltage was applied between the AFM tip and a silver contact localized at the poly-Si(B) surface), with and without SiO<sub>x</sub> layer at the poly-Si/c-Si interface ( $T_a = 700^\circ\text{C}$ ). C-AFM measurements were performed with a delay of 5h after HF-cleaning the samples' surface. Resulting current maps are depicted in Fig. 9. The current maps showed conductive spots ( $> 1 \text{ nA}$ ) with a density of  $24.9 \mu\text{m}^{-2}$  and  $11.2 \mu\text{m}^{-2}$  with and without SiO<sub>x</sub> respectively. The current levels detected on the sample with interfacial SiO<sub>x</sub> (Fig. 9a) were slightly higher than the ones detected without SiO<sub>x</sub> layer (Fig. 9b) which is consistent with the transversal C-AFM measurements on similar samples (Fig. 8a and 8c respectively) and supports the hypothesis that it is related to change in the conduction properties of the poly-Si layer. The lower current levels and lower conductive spots densities detected in lateral configuration (Fig. 9) compared to measurements in transversal configuration (Fig. 8) are resulting from the longer delay between the samples HF-cleaning and the lateral measurements (measured 3h later). A qualitative comparison of the lateral and transversal current maps is nevertheless possible. One can notice a similar current pattern in both configurations although in lateral configuration, the current is expected to flow principally in the poly-Si layer. These observations suggest that the conductive spots observed on C-AFM current maps are linked to the poly-Si microstructure rather than mirroring pinholes in the SiO<sub>x</sub> layer. Conductive spots could be the result of a different local conduction in the poly-Si layer, e.g. the crystalline grains would conduct differently than the grain boundaries (or remaining amorphous phases), as it was observed in ref. [49].

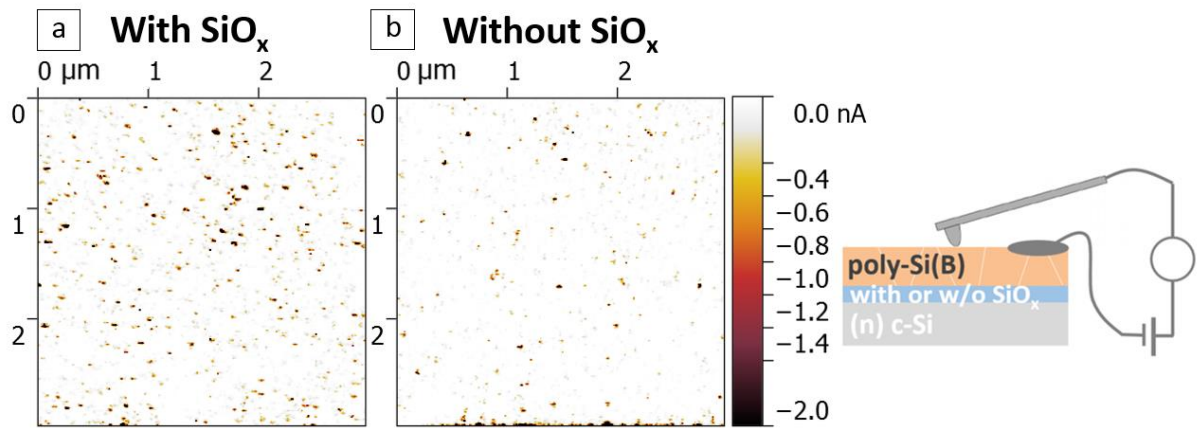


Fig. 9. Current maps obtained by C-AFM measurement in lateral configuration on 20 nm-thick poly-Si(B) layers ( $T_a = 700^\circ\text{C}$ ) with (a) and without (b)  $\text{SiO}_x$  layer at the poly-Si(B)/(n)c-Si interface. C-AFM measurements were performed 5h after HF-cleaning the samples' surface to ensure a similar surface state during both measurements.

#### 4. Conclusion

In conclusion, we presented highly passivating and blister-free poly-Si(B)/ $\text{SiO}_x$  structures fabricated by PECVD with the aim of passivating c-Si solar cell contacts. First, the blistering issue appearing because of the high H content of the a-Si:H deposited layer was overcome by optimizing the deposition temperature and gas ratio. For poly-Si(B)/ $\text{SiO}_x$  structures made on KOH-polished 156 psq c-Si wafers, the surface passivation properties were further improved by addition of a hydrogenation step leading to a maximum  $iV_{oc}$  value of 734 mV.

The poly-Si(B)/ $\text{SiO}_x$  samples were then studied by means of C-AFM with the aim of investigating the formation of conductive pinholes in the  $\text{SiO}_x$  layer. We showed that the growth of an oxide at the poly-Si top surface affects the current levels detected by C-AFM. We observed similar C-AFM current patterns in transversal configuration on samples with and without interfacial  $\text{SiO}_x$  layer as well as in lateral configuration where the current is expected to flow principally in the poly-Si layer. These observations disprove the hypothesis that conductive spots detected by C-AFM would mirror pinholes within the  $\text{SiO}_x$  layer but rather suggest that the conductive spots would relate to the poly-Si microstructure.

## Funding

This work was supported by the French National Research Agency (Programs “Investment for the Future” ANR-IEED-002-01, ANR-10-ITE-0003 and “Oxygen” ANR-17-CE05-0035) and has also received funding from the European Union’s Horizon 2020 research and innovation program under grant agreement No 727529.

## References

- [1] T. Dullweber, J. Schmidt, Industrial Silicon Solar Cells Applying the Passivated Emitter and Rear Cell (PERC) Concept—A Review, *IEEE J. Photovolt.* 6 (2016) 1366–1381. doi:10.1109/JPHOTOV.2016.2571627.
- [2] S.W. Glunz, F. Feldmann, A. Richter, M. Bivour, C. Reichel, H. Steinkemper, J. Benick, M. Hermle, The irresistible charm of a simple current flow pattern - 25% with a solar cell featuring a full-area back contact, *Proc. 31st Eur. Photovolt. Sol. Energy Conf. Exhib.* (2015) Hamburg, Germany.
- [3] D. Adachi, J.L. Hernández, K. Yamamoto, Impact of carrier recombination on fill factor for large area heterojunction crystalline silicon solar cell with 25.1% efficiency, *Appl. Phys. Lett.* 107 (2015) 233506. doi:10.1063/1.4937224.
- [4] S. De Wolf, A. Descoeurdes, Z.C. Holman, C. Ballif, High-efficiency Silicon Heterojunction Solar Cells: A Review, *Green.* 2 (2012). doi:10.1515/green-2011-0018.
- [5] U. Römer, R. Peibst, T. Ohrdes, B. Lim, J. Krügener, E. Bugiel, T. Wietler, R. Brendel, Recombination behavior and contact resistance of n+ and p+ poly-crystalline Si/mono-crystalline Si junctions, *Sol. Energy Mater. Sol. Cells.* 131 (2014) 85–91. doi:10.1016/j.solmat.2014.06.003.
- [6] F. Feldmann, C. Reichel, R. Müller, M. Hermle, The application of poly-Si/SiO<sub>x</sub> contacts as passivated top/rear contacts in Si solar cells, *Sol. Energy Mater. Sol. Cells.* 159 (2017) 265–271. doi:10.1016/j.solmat.2016.09.015.
- [7] M.K. Stodolny, J. Anker, B. Geerligs, G.J.M. Janssen, B.W.H. van de Loo, J. Melskens, R. Santbergen, O. Isabella, J. Schmitz, M. Lenes, J.-M. Luchies, W.M.M. Kessels, I. Romijn, Material properties of LPCVD processed n-type polysilicon passivating contacts and its application in PERPoly industrial bifacial solar cells, *Energy Procedia.* (2017) 635–642.
- [8] F. Feldmann, M. Bivour, C. Reichel, M. Hermle, S.W. Glunz, Passivated rear contacts for high-efficiency n-type Si solar cells providing high interface passivation quality and excellent transport characteristics, *Sol. Energy Mater. Sol. Cells.* 120 (2014) 270–274. doi:10.1016/j.solmat.2013.09.017.
- [9] Y. Larionova, M. Turcu, S. Reiter, R. Brendel, D. Tetzlaff, J. Krügener, T. Wietler, U. Höhne, J.-D. Kähler, R. Peibst, On the recombination behavior of p<sup>+</sup>-type polysilicon on oxide junctions deposited by different methods on textured and planar surfaces: On the recombination behavior of p<sup>+</sup>-type polysilicon on oxide junctions, *Phys. Status Solidi A.* 214 (2017) 1700058. doi:10.1002/pssa.201700058.
- [10] Y. Tao, V. Upadhyaya, Y.-Y. Huang, C.-W. Chen, K. Jones, A. Rohatgi, Carrier selective tunnel oxide passivated contact enabling 21.4% efficient large-area n-type silicon solar cells, in: *Photovolt. Spec. Conf. PVSC 2016 IEEE 43rd, IEEE*, 2016: pp. 2531–2535.
- [11] B. Nemeth, D.L. Young, M.R. Page, V. LaSalvia, S. Johnston, R. Reedy, P. Stradins, Polycrystalline silicon passivated tunneling contacts for high efficiency silicon solar cells, *J. Mater. Res.* 31 (2016) 671–681. doi:10.1557/jmr.2016.77.
- [12] G. Nogay, J. Stuckelberger, P. Wyss, E. Rucavado, C. Allebé, T. Koida, M. Morales-Masis, M. Despeisse, F.-J. Haug, P. Löper, C. Ballif, Interplay of annealing temperature and doping in hole

- selective rear contacts based on silicon-rich silicon-carbide thin films, *Sol. Energy Mater. Sol. Cells.* 173 (2017) 18–24. doi:10.1016/j.solmat.2017.06.039.
- [13] N. Nandakumar, J. Rodriguez, T. Kluge, T. Große, L. Fondop, P. Padhamnath, N. Balaji, M. König, S. Duttagupta, Approaching 23% with large-area monoPoly cells using screen-printed and fired rear passivating contacts fabricated by inline PECVD, *Prog. Photovolt. Res. Appl.* (2018). doi:10.1002/pip.3097.
- [14] D. Yan, A. Cuevas, S.P. Phang, Y. Wan, D. Macdonald, 23% efficient p-type crystalline silicon solar cells with hole-selective passivating contacts based on physical vapor deposition of doped silicon films, *Appl. Phys. Lett.* 113 (2018) 61603. doi:10.1063/1.5037610.
- [15] U. Romer, R. Peibst, T. Ohrdes, B. Lim, J. Krugener, T. Wietler, R. Brendel, Ion Implantation for Poly-Si Passivated Back-Junction Back-Contacted Solar Cells, *IEEE J. Photovolt.* 5 (2015) 507–514. doi:10.1109/JPHOTOV.2014.2382975.
- [16] D.L. Young, W. Nemeth, V. LaSalvia, M.R. Page, S. Theingi, J. Aguiar, B.G. Lee, P. Stradins, Low-cost plasma immersion ion implantation doping for Interdigitated back passivated contact (IBPC) solar cells, *Sol. Energy Mater. Sol. Cells.* 158 (2016) 68–76. doi:10.1016/j.solmat.2016.05.044.
- [17] F. Feldmann, M. Simon, M. Bivour, C. Reichel, M. Hermle, S.W. Glunz, Efficient carrier-selective p- and n-contacts for Si solar cells, *Sol. Energy Mater. Sol. Cells.* 131 (2014) 100–104. doi:10.1016/j.solmat.2014.05.039.
- [18] A. Richter, J. Benick, F. Feldmann, A. Fell, M. Hermle, S.W. Glunz, n-Type Si solar cells with passivating electron contact: Identifying sources for efficiency limitations by wafer thickness and resistivity variation, *Sol. Energy Mater. Sol. Cells.* 173 (2017) 96–105. doi:10.1016/j.solmat.2017.05.042.
- [19] F. Haase, C. Klamt, S. Schäfer, A. Merkle, M. Rienäcker, J. Krügener, R. Brendel, R. Peibst, Laser contact openings for local poly-Si-metal contacts, *Silicon PV 2018.* (2018) Lausanne, Switzerland.
- [20] G. Nogay, A. Ingenito, E. Rucavado, Q. Jeangros, J. Stuckelberger, P. Wyss, M. Morales-Masis, F.-J. Haug, P. Loper, C. Ballif, Crystalline Silicon Solar Cells With Coannealed Electron- and Hole-Selective SiC  $\text{SiC}$  Passivating Contacts, *IEEE J. Photovolt.* (2018) 1–8. doi:10.1109/JPHOTOV.2018.2866189.
- [21] S. Mack, J. Schube, T. Fellmeth, F. Feldmann, M. Lenes, J.-M. Luchies, Metallisation of Boron-Doped Polysilicon Layers by Screen Printed Silver Pastes, *Phys. Status Solidi RRL - Rapid Res. Lett.* 11 (2017) 1700334. doi:10.1002/pssr.201700334.
- [22] A. Mewe, M. Stodolny, J. Anker, M. Lenes, X. Pagès, Y. Wu, K. Tool, B. Geerligs, I. Romijn, Full wafer size IBC cell with polysilicon passivating contacts, in: *Lausanne, Switzerland, 2018:* p. 40014. doi:10.1063/1.5049277.
- [23] D.L. Young, B.G. Lee, D. Fogel, W. Nemeth, V. LaSalvia, S. Theingi, M. Page, M. Young, C. Perkins, P. Stradins, Gallium-Doped Poly-Si:Ga/SiO<sub>2</sub> Passivated Emitters to n-Cz Wafers With  $V_{oc} > 730$  mV, *IEEE J. Photovolt.* 7 (2017) 1640–1645. doi:10.1109/JPHOTOV.2017.2748422.
- [24] T. Yamamoto, K. 'ichi Uwasawa, T. Mogami, Bias temperature instability in scaled p<sup>+</sup>/polysilicon gate p-MOSFET's, *IEEE Trans. Electron Devices.* 46 (1999) 921–926.
- [25] R.B. Fair, Physical models of boron diffusion in ultrathin gate oxides, *J. Electrochem. Soc.* 144 (1997) 708–717.
- [26] I. Mack, J. Stuckelberger, P. Wyss, G. Nogay, Q. Jeangros, J. Horzel, C. Allebé, M. Despeisse, F.-J. Haug, A. Ingenito, P. Löper, C. Ballif, Properties of mixed phase silicon-oxide-based passivating contacts for silicon solar cells, *Sol. Energy Mater. Sol. Cells.* 181 (2018) 9–14. doi:10.1016/j.solmat.2017.12.030.
- [27] F. Feldmann, G. Nogay, P. Löper, D.L. Young, B.G. Lee, P. Stradins, M. Hermle, S.W. Glunz, Charge carrier transport mechanisms of passivating contacts studied by temperature-dependent J-V measurements, *Sol. Energy Mater. Sol. Cells.* 178 (2018) 15–19. doi:10.1016/j.solmat.2018.01.008.
- [28] N. Folchert, M. Rienäcker, A.A. Yeo, B. Min, R. Peibst, R. Brendel, Temperature-dependent contact resistance of carrier selective Poly-Si on oxide junctions, *Sol. Energy Mater. Sol. Cells.* 185 (2018) 425–430. doi:10.1016/j.solmat.2018.05.046.

- [29] F. Feldmann, G. Nogay, J.-I. Polzin, B. Steinhauser, A. Richter, A. Fell, C. Schmiga, M. Hermle, S.W. Glunz, A Study on the Charge Carrier Transport of Passivating Contacts, *IEEE J. Photovolt.* (2018) 1–7. doi:10.1109/JPHOTOV.2018.2870735.
- [30] S.W. Glunz, F. Feldmann, SiO<sub>2</sub> surface passivation layers – a key technology for silicon solar cells, *Sol. Energy Mater. Sol. Cells.* 185 (2018) 260–269. doi:10.1016/j.solmat.2018.04.029.
- [31] A.S. Kale, W. Nemeth, H. Guthrey, E. Kennedy, A.G. Norman, M. Page, M. Al-Jassim, D.L. Young, S. Agarwal, P. Stradins, Understanding the charge transport mechanisms through ultrathin SiO<sub>x</sub> layers in passivated contacts for high-efficiency silicon solar cells, *Appl. Phys. Lett.* 114 (2019) 83902. doi:10.1063/1.5081832.
- [32] H. Steinkemper, F. Feldmann, M. Bivour, M. Hermle, Numerical Simulation of Carrier-Selective Electron Contacts Featuring Tunnel Oxides, *IEEE J. Photovolt.* 5 (2015) 1348–1356. doi:10.1109/JPHOTOV.2015.2455346.
- [33] R. Peibst, U. Römer, Y. Larionova, M. Rienäcker, A. Merkle, N. Folchert, S. Reiter, M. Turcu, B. Min, J. Krügener, D. Tetzlaff, E. Bugiel, T. Wietler, R. Brendel, Working principle of carrier selective poly-Si/c-Si junctions: Is tunnelling the whole story?, *Sol. Energy Mater. Sol. Cells.* 158 (2016) 60–67. doi:10.1016/j.solmat.2016.05.045.
- [34] K. Lancaster, S. Großer, F. Feldmann, V. Naumann, C. Hagendorf, Study of Pinhole Conductivity at Passivated Carrier-selected Contacts of Silicon Solar Cells, *Energy Procedia.* 92 (2016) 116–121. doi:10.1016/j.egypro.2016.07.040.
- [35] Z. Zhang, Y. Zeng, C.-S. Jiang, Y. Huang, M. Liao, H. Tong, M. Al-Jassim, P. Gao, C. Shou, X. Zhou, B. Yan, J. Ye, Carrier transport through the ultrathin silicon-oxide layer in tunnel oxide passivated contact (TOPCon) c-Si solar cells, *Sol. Energy Mater. Sol. Cells.* 187 (2018) 113–122. doi:10.1016/j.solmat.2018.07.025.
- [36] G.E. Jellison, M.F. Chisholm, S.M. Gorbalkin, Optical functions of chemical vapor deposited thin-film silicon determined by spectroscopic ellipsometry, *Appl. Phys. Lett.* 62 (1993) 3348–3350. doi:10.1063/1.109067.
- [37] D.E. Kane, R.M. Swanson, Measurement of the emitter saturation current by a contactless photoconductivity decay method (silicon solar cells), *Conf. Rec. IEEE Photovolt. Spec. Conf.* (1985) 578–583.
- [38] J.A. Aguiar, D. Young, B. Lee, W. Nemeth, S. Harvey, T. Aoki, M. Al-Jassim, P. Stradins, Atomic scale understanding of poly-Si/SiO<sub>2</sub>/c-Si passivated contacts: Passivation degradation due to metallization, in: *Photovolt. Spec. Conf. PVSC 2016 IEEE 43rd*, IEEE, 2016: pp. 3667–3670.
- [39] S. De Wolf, M. Kondo, Nature of doped a-Si:H/c-Si interface recombination, *J. Appl. Phys.* 105 (2009) 103707. doi:10.1063/1.3129578.
- [40] R.A. Street, *Hydrogenated amorphous silicon*, Cambridge University Press, Cambridge, England, 1991.
- [41] C. Voz, D. Peiro, J. Bertomeu, D. Soler, M. Fonrodona, J. Andreu, Optimisation of doped microcrystalline silicon films deposited at very low temperatures by hot-wire CVD, *Mater. Sci. Eng. B.* 69–70 (2000) 278–283.
- [42] F. Lebreton, S.N. Abolmasov, F. Silva, P. Roca i Cabarrocas, *In situ* photoluminescence study of plasma-induced damage at the a-Si:H/c-Si interface, *Appl. Phys. Lett.* 108 (2016) 51603. doi:10.1063/1.4941298.
- [43] B.E. Deal, The current understanding of charges in the thermally oxidized silicon structure, *J. Electrochem. Soc.* 121 (1974) 198C–205C.
- [44] R. Brendel, R. Peibst, Contact selectivity and efficiency in crystalline silicon photovoltaics, *IEEE J. Photovolt.* 6 (2016) 1413–1420.
- [45] A.S. Kale, W. Nemeth, S.P. Harvey, M. Page, D.L. Young, S. Agarwal, P. Stradins, Effect of silicon oxide thickness on polysilicon based passivated contacts for high-efficiency crystalline silicon solar cells, *Sol. Energy Mater. Sol. Cells.* 185 (2018) 270–276. doi:10.1016/j.solmat.2018.05.011.
- [46] G.R. Wolstenholme, N. Jorgensen, P. Ashburn, G.R. Booker, An investigation of the thermal stability of the interfacial oxide in polycrystalline silicon emitter bipolar transistors by comparing device results with high-resolution electron microscopy observations, *J. Appl. Phys.* 61 (1987) 225–233. doi:10.1063/1.338861.



- [47] S. Choi, K.H. Min, M.S. Jeong, J.I. Lee, M.G. Kang, H.-E. Song, Y. Kang, H.-S. Lee, D. Kim, K.-H. Kim, Structural evolution of tunneling oxide passivating contact upon thermal annealing, *Sci. Rep.* 7 (2017). doi:10.1038/s41598-017-13180-y.
- [48] D. Tetzlaff, J. Krügener, Y. Larionova, S. Reiter, M. Turcu, F. Haase, R. Brendel, R. Peibst, U. Höhne, J.-D. Kähler, T.F. Wietler, A simple method for pinhole detection in carrier selective POLO-junctions for high efficiency silicon solar cells, *Sol. Energy Mater. Sol. Cells.* 173 (2017) 106–110. doi:10.1016/j.solmat.2017.05.041.
- [49] O. Shamiryanyan, I. Maidanchuk, N. Ahn, I. Choi, C.H. Kyoonyoung, Electrical characterization of thin silicon films produced by metal-induced crystallization on insulating substrates by conductive AFM, *J. Surf. Anal.* 17 (2011) 260–263.